AD-A081 724 NAVAL RESEARCH LAB WASHINGTON DC F/G 20/9
TRANSIENT FIELD REVERSAL WITH A PROTON LAYER.(U)
DEC 79 C A KAPETANAKOS, J GOLDEN, J A PASOUR
UNCLASSIFIED NRL-MR-4135 SBIE-AD-E000 371 NL

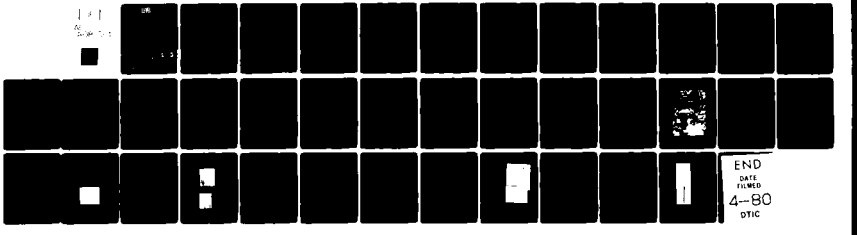

END
DATE FILMED
4-80
DTIC

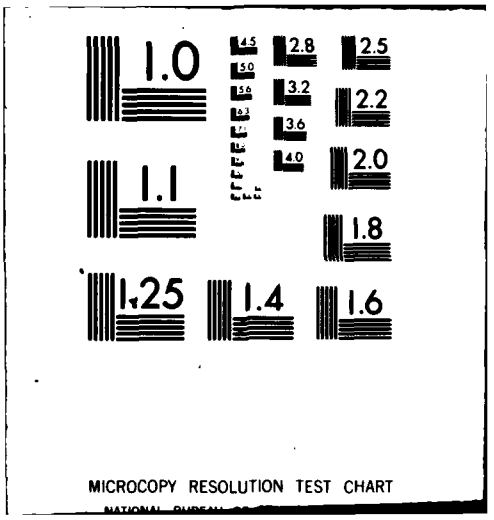
1.0
1.1
1.25
1.4
1.6
1.8
2.0
2.2
2.5
2.8
3.2
3.6
4.0
4.5
5.0
5.6
6.3
MICROCOPY RESOLUTION TEST CHART

(12) LEVEL III

(19) AD-E 000 377

(14) NRL-MR-

(18) SBIE

(9) NRL Memorandum Report 4135

ADA081724

(6) Transient Field Reversal with a Proton Layer.

(10) C. A. KAPETANAKOS, J. GOLDEN, T. A. PASOUR

~~Experimental Plasma Physics Branch~~
~~Plasma Physics Division~~

S. J. MARSH and R. A. MAHAFFEY

Sachs-Freeman Associates, Inc.
Bladensburg, Maryland 20710

(12) 38

(11) 27 December 1979

(16) RR011099

(17) RR011109441

251950

NAVAL RESEARCH LABORATORY
Washington, D.C.

SECURITY CLASSIFICATION OF THIS PAGE (When Data Entered)

REPORT DOCUMENTATION PAGE

READ INSTRUCTIONS BEFORE COMPLETING FORM

1. REPORT NUMBER: NRL Memorandum Report 4135	2. GOVT ACCESSION NO.
3. RECIPIENT'S CATALOG NUMBER	
4. TITLE (and Subtitle): TRANSIENT FIELD REVERSAL WITH A PROTON LAYER	5. TYPE OF REPORT & PERIOD COVERED: Interim report on a continuing NRL problem.
6. PERFORMING ORG. REPORT NUMBER	
7. AUTHOR(s): C. A. Kapetanakos, J. Golden, J. A. Pasour, S. J. Marsh* and R. A. Mahaffey*	8. CONTRACT OR GRANT NUMBER(s)
9. PERFORMING ORGANIZATION NAME AND ADDRESS: Naval Research Laboratory, Washington, DC 20375	10. PROGRAM ELEMENT, PROJECT, TASK AREA & WORK UNIT NUMBERS: NRL Problem 67-0869-0-0
11. CONTROLLING OFFICE NAME AND ADDRESS: Office of Naval Research, Arlington, Virginia 22217	12. REPORT DATE: December 27, 1979
	13. NUMBER OF PAGES: 37
14. MONITORING AGENCY NAME & ADDRESS(if different from Controlling Office)	15. SECURITY CLASS. (of this report): UNCLASSIFIED
	15a. DECLASSIFICATION/DOWNGRADING SCHEDULE

16. DISTRIBUTION STATEMENT (of this Report)

Approved for public release; distribution unlimited.

17. DISTRIBUTION STATEMENT (of the abstract entered in Block 20, if different from Report)

18. SUPPLEMENTARY NOTES

*Sachs-Freeman Associates, Inc., Bladensburg, Maryland 20710

This research was supported by the Department of Energy and the Office of Naval Research.

19. KEY WORDS (Continue on reverse side if necessary and identify by block number)

Field reversed configurations
Ion rings
Intense proton beams

20. ABSTRACT (Continue on reverse side if necessary and identify by block number)

This report describes a series of experiments that led to the transient field reversal of the applied magnetic field with a proton pulse. The 400-500 KA, 50 nsec duration, 1.7 MeV peak energy hollow proton pulse is generated by an Inverse Reflex Tetrode. After passing through the cusp, the pulse propagates in a uniform field with 1.15 cm/nsec axial velocity, when the applied voltage on the anode is 1MV.

DD FORM 1 JAN 73 1473 EDITION OF 1 NOV 65 IS OBSOLETE
S/N 0102-014-6601

SECURITY CLASSIFICATION OF THIS PAGE (When Data Entered)

CONTENTS

1. Introduction

Magnetic field configurations with closed field lines generated by energetic particles are very promising for confining plasmas for thermonuclear applications for the following four main reasons: (1) the plasma confinement time is considerably enhanced because the trapped plasma would have to cross the closed magnetic field lines in order to escape; (2) the gyrating particles of the ring serve as an internal energy source for heating the confined plasma; (3) the closed minimum-B magnetic field configuration provides hydrodynamical stability to the plasma; and (4) the beta of the plasma can exceed unity[1] and thus the power density of a thermonuclear reactor can be high. As a result, the reactor can have a small size resulting in very significant economic benefits.

Initially, as a consequence of the availability of high current relativistic electron beams, the effort was focused on the formation of relativistic electron layers.[2-4] However, reversed field configurations that are generated by energetic electrons are not of interest for thermonuclear applications because of the synchrotron radiation losses from the fast moving electrons. To avoid the radiation losses Christofilos[5] proposed the replacement of electrons by ions having energies in the GeV range. In Christofilos scheme, as well as in a similar scheme proposed by McNally[6], the ion beams are generated by conventional accelerators and have very low current (~1mA).

Another way to create a reversed magnetic field configuration with energetic particles is by the tangential injection of neutral beams. Diamagnetic

Note: Manuscript submitted November 20, 1979.

signals approaching the applied magnetic field have been obtained with this technique in the 2X11B facility at Livermore by Simonen et al.[7].

Although field reversal has not been achieved as yet by the tangential injection of neutral beams, the recent technological advances[8-14] in the generation of intense, pulsed ion sources made possible recently the transient field reversal[15] of the applied magnetic field by a short proton layer at the Naval Research Laboratory. These results demonstrate that the formation of a trapped, field reversed ion ring is within the capabilities of the existing pulsed-power technology.

This report describes a series of experiments that led to the first field reversal ever achieved with ions. In these experiments the applied magnetic field consists of a short uniform region, in which the ion source is located, a magnetic cusp, a 75 cm long uniform field and a half mirror. About 8×10^{16} protons per pulse are generated by an Inverse Reflex Tetrode[11] (IRT) ion source that is powered by the Gamble II generator. The peak proton current is 400 - 500 kA when the ramp shaped (corrected) voltage that is applied to the anode of the IRT increases from 0.6 MV to 1.7 MV within 50 nsec. As a result of the ramp-shaped voltage and the somersault effect[16], the ion pulse bunches axially thus generating self fields that exceed the applied field. Magnetic probes that are located in the 1.5 kG, 75 cm long field plateau along the axis of the system show that the rotating ion pulse reverses the external field. The field reversal factor exceeds 120%. In addition, the signals of magnetic probes show that the ion pulse propagates with an axial speed v_z which is 1.1 - 1.2 cm/nsec,

when the applied peak voltage on the anode is about 1 MV. The mean velocity of rotation v_θ is only 1/5 of v_z. Currently, experiments are in progress to increase the ratio v_θ/v_z and to trap the ion pulse in a gated magnetic mirror field.

2. Description of the Experiment

A schematic of the experiment that does not include the gate coil and the magnetic mirror is shown in Fig. 1. A photograph of the same section is shown in Fig. 2. The applied magnetic field that is used in the experiments described in this report is shown in Fig. 3. It consists of a short uniform region, a magnetic cusp, a 75 cm long uniform field and a single magnetic mirror. The Inverse Reflex Tetrode (IRT) ion source shown in Fig. 4 is located in the short uniform field and is powered by the upgraded Gamble II generator. The low inductance ion source has a 75 cm long, 33 cm outside diameter cylindrical anode stalk. The 100μm thick, 18.5 cm i.d. hollow polyethylene anode foil (A) is mounted on the front end of the anode stalk. The other end of the stalk is covered by a thin stainless steel plate. Electrically connected to the end plate is a movable stainless steel disc (G). Electrons emitted from the grounded screen cathode (K) are accelerated toward the semitransparent anode, pass through it and form a virtual cathode VC between A and G. Those electrons transmitted through the VC reach the grid G. The rest of the electrons oscillate between the virtual and real cathode, until they are absorbed by the anode. The protons are extracted out of the plasma that is formed from the plastic anode. When the applied voltage increases or remains constant, protons directed toward the virtual cathode are unable to reach the grid or they

reach it with zero velocity. Thus, these protons do not deplete the energy content of the system. However, most of those ions emitted toward K pass through the coarse screen and enter the cusp.

In the absence of ions and in the presence of a strong magnetic field the electron current reaching the grid can be computed from[17]

$$I_\ell = \frac{17(\gamma_o^{2/3} - 1)^{3/2}}{1 + 2\ell n\ (R/a_o)} \quad KA, \tag{1}$$

where a_o is the electron beam radius, R is the radius of the anode stalk and γ_o is the relativistic factor. For $R \approx a_o$ and $\gamma_o = 3$, Eq. (1) gives $I_\ell \approx 19$ KA. However, in practice I_ℓ is appreciably higher because the electron space charge is partially neutralized by the ions.

The axial distance ℓ of the center of the virtual cathode from the anode may be estimated from[18]

$$\frac{I_{inj}}{I_\ell} \approx \{1 - e^{-2.4(\ell/R)}\}^{-2}, \tag{2}$$

where I_{inj} is the injected electron current. For R = 15 cm and $I_\ell/I_{inj} = 1/20$, Eq. (2) gives $\ell = 1.5$ cm. Equation (2) has been derived neglecting the ions and the effect of the end plate G. This effect can be neglected provided[17,19]

$$L/R \geq 2.5\ (a_o/R)^{0.133},$$

where L is the A-G axial distance.

The importance of A-G separation in the formation of the virtual cathode is demonstrated in Fig. 5. The solid line shows the potential

on axis $\phi(0,z)$ inside a biased (V = 500 kV) conducting cylindrical box of radius R = 5 cm, bounded by two conducting plates that are 5 cm apart, in the presence of two solid electron beams of radius a_o = 2.5 cm. One of these beams of density $n_1 = 2 \times 10^{11}$ cm^{-3} extends from z = 0 to the virtual cathode and the second of density $n_2 = 1.28 \times 10^{11}$ cm^{-3} extends from the virtual cathode to the back plate (z = L). The dashed line shows the potential when the spacing between the two end plates is reduced to 2.5 cm. Clearly, no virtual cathode is formed.

Pinhole x-ray photographs (Fig. 6) of two lead wires located inside the cylindrical anode box 15-cm from the anode show that the oscillating hollow electron beam does not pinch even in the absence of an applied magnetic field. The observed "filling-in" is probably associated with the $v_z B_\theta$ force, the radial space charge electric field and the scattering of the electrons in the anode foil.

For a limited range of relevant parameters (applied voltage, anode thickness, applied magnetic field), the IRT has the interesting features that its impedance (Z) remains approximately constant during an appreciable fraction of the 80 nsec long pulse. This is shown in Fig. 7. A consequence of $Z \approx$ const. is that the inductively corrected voltage at the anode increases with time. Typically, after a fast initial rise, the voltage increases from 0.6 MV to about 1.7 MV within 60 nsec. Such a voltage waveform is shown in Fig. 8, together with the total voltage, total current I and dI/dt.

Another consequence of $Z \approx$ const, is that the ion source is coupled to the generator with high efficiency. Figure 9 shows that approximately

75 KJ of energy are extracted out of the generator, i.e., approximately 85% of the maximum energy delivered to a matched load. The peak power delivered by the generator to the ion source (Fig. 10) is approximately 1.4 TW.

3. Results

The number of protons[20] at various axial positions, is inferred from the measured number of delayed γ rays emitted from the annihilation of positrons ($\beta+$) that are produced in the resonant reaction $^{12}C(p,\gamma)^{13}N(\beta+)^{13}C$. In the coincidence counting the only γ rays recorded are those with energy near 0.5 MeV. The number of counts is corrected for the reaction $^{12}C(d,n)^{13}N(\beta+)^{13}C$ induced by the natural isotopic abundance of deuterium in polyethylene. In our best shots the total number of protons measured with the carbon target located 15 cm from the anode is between 7×10^{16} to 8×10^{16} per pulse. This number must be considered as a lower bound since protons with energy less than 470 keV do not activate the target and the number of counts is not corrected for target blowoff. For a triangular ion pulse of 50 nsec base line duration the 8×16^{16} particles correspond to 500 kA peak proton current.

The radial profile of the beam is determined by individually counting small segments of a carbon target after it is activated by the beam. Figure 11 shows the radial profile of the proton beam 15 cm from the anode. It is apparent that the thickness of the beam is appreciably greater than that of the anode foil. The observed "filling-in" of the proton beams is due mainly to the $v_z B_\theta$ pinching force that acts on the ions inside the anode-cathode gap. The azimuthal magnetic

field B_θ is generated by the ion current and the net electron current in the gap. It is estimated from the equations of motion, neglecting the radial electric fields, that at the cathode the protons have a radial velocity $v_r = v \sin\theta$, where v is the velocity corresponding to the applied voltage and

$$\text{Sin } \theta \approx (d/\tau V_o) \int_o^d B_\theta \, dz. \qquad (3)$$

In Eq. (3) d is anode-cathode gap, τ is the transit time of the ions, V_o the applied voltage on the anode and the integral is along the particle orbit. For d = 2 cm, $B_\theta = 10^4$ Gauss = const., V_o = 1 MV, Eq. (3) gives $\theta \approx 16^o$.

The beam current is inferred from the prompt γ-ray flux emitted from the reaction $^{19}F(p,\alpha\gamma)^{16}O$, when the proton beam strikes a telfon target[21]. This technique has the advantage that the error resulting from the target blow-off is insignificant. Unfortunately, this diagnostic technique cannot be readily used to measure the proton current near the source because of the copious burst of x-rays that is produced in the IRT by the high energy electrons. However, when the target is separated from the source by a long distance so that the time of flight of the protons is greater than the duration of the voltage pulse, the interference of the bremsstrahlung is eliminated. A typical trace obtained when the teflon target is located 145 cm from the cusp is shown in Fig. 12. The first peak is due to bremsstrahlung and the second to the prompt γrays. The detector has been calibrated using a Van de Graaff accelerator. However, the proton current has not been determined, as yet, by this technique because of the incomplete information on the energy distribution of the protons near the target.

The magnetic field is monitored with several fast, center tapped magnetic probes. After integration, the signal from each half of the probe is fed to the differential amplifier of an oscilloscope. A three-coil probe is inserted from the downstream end of the system along the symmetry axis and monitors the axial magnetic field ΔB_z at 10 cm, 60 cm and 110 cm from the cusp. Typical oscilloscope traces from this multi-probe are shown in Fig. 13. The second probe is located in the uniform external magnetic field and the peak of the signal is 1.25 times greater than the applied magnetic field, i.e., the external field has been reversed. The peak of the third trace is lower than the peak of the second perhaps as a consequence of particle losses on the converging walls of the vacuum chamber. The low level signal that precedes the main signal in the third trace is extraneous and does not change polarity when the external field is reversed. Although all of the signals of the magnetic probes that are located at r = 0 are diamagnetic, the polarity of the trace at the top of Fig. 13 has been reversed at the oscilloscope for display purposes.

It has been determined from the time delay between the signals of B_{z2} and B_{z3} probes that in the uniform field the rotating layer propagates with an average axial velocity of about 1.15 cm/nsec, when the applied voltage on the anode is approximately 1 MV. The solid line in Fig. 14 shows the dependence of the measured axial velocity upon the applied peak voltage. The dashed line gives the computed velocity corresponding to the applied voltage. The vertical separation between the two lines accounts for the energy of the particles perpendicular

to the field as well as for the energy invested to build-up the self magnetic field.

The macroscopic velocity of rotation v_θ of the ion pulse is inferred from the measured rotation of the image of a discontinuity introduced to the pulse by a mask and the known distance between the target and the mask. Typically, $v_\theta \approx v_z/5$. Therefore, when the applied voltage is about 1 MV the energy associated with the azimuthal rotation is approximately 40 keV. The gyroradius of a proton with this energy in a 1.5 KG magnetic field is about 19 cm. This radius is further reduced because of the compression of the self magnetic field by the wall of the vacuum chamber. From the temporal half maximum width of the prompt γ-ray pulse that is typically 25 nsec (Fig. 12) and the measured axial velocity, it is estimated that the length of the ion pulse is about 27 cm when the peak applied voltage is 1 MV. A similar conclusion can be reached from the temporal widths and the time delay of the signals of the B_z probes that are located near the wall of the chamber.

The radial profile of the beam at 145 cm after the cusp measured with the activation technique using segmented carbon targets is shown in Fig. 15. It is evident from this figure that the particle density of the pulse is peaked a few centimeters from the symmetry axis of the system.

At this point, it is necessary to examine if the observed diamagnetic signal of the pulse is consistent with the observed approximate dimensions, velocity and total number of protons. Table I gives the azimuthal current required to generate a 1.8 KG magnetic field at the center of a coil of length 2L, inner radius a_1 and outer radius a_2,

when the current density is uniform. For a_1 = 5 cm, a_2 = 15 cm, 2L = 30 cm, the azimuthal current is 52 KA, i.e., about 1/8 of the total proton current of the ion source and in agreement with the ratio v_θ/v_z 1/5.

Additional insight is gained by considering a long rigidly rotating ion layer. If a_1 is the inner and a_2 the outer radius of a space charge neutral layer that rotates with a constant angular frequency ω around its axis of symmetry, the ratio of the total magnetic field in the interior of the layer $\{a_1 \leq r \leq a_2\}$ to the applied magnetic field B_o is given by[22]

$$\frac{B_z(r)}{B_o} = 1 + \frac{2\omega\nu}{\Omega_o}\left[\frac{(a_2^2 - r^2)}{(a_2^2 - a_1^2)} - \frac{(a_1^2 + a_2^2)}{2b^2}\right], \qquad (4)$$

where $\Omega_o = \frac{qB_o}{mc}$ is the cyclotron frequency corresponding to the applied field, q and m are the charge and mass of gyrating particles, $\nu\{ = N_\ell R_o$, where N_ℓ is the number of ions per unit length and R_o is the ion classical radius $\}$ is the Budker parameter and b is the radius of a perfectly conducting wall that surrounds the layer. The magnetic field for $r \leq a_1$ and $a_2 \leq r \leq b$ is constant and may be found by letting $r = a_1$ and $r = a_2$ in Eq. (4) respectively. The last term in Eq. (4) is due to induced currents (eddy currents) on the wall of the conducting cylinder surrounding the layer and becomes zero when the conductor is removed ($b \to \infty$).

The field reversal factor $\eta = B_z(a_1)/B_o$ may be found from Eq. (4) by letting $r = a_1$ and using the relation $\Omega(\rho) = \frac{qB_z(\rho)}{mc} = -\omega$, where $\rho^2 = (a_1^2 + a_2^2)/2$. After some simple algebra, it is obtained that $\eta = \frac{|\omega|}{\Omega_o}(1-\nu)$. Therefore, field reversal ($\eta \leq 0$) requires a Budker parameter that exceeds unity, i.e., $N_\ell \geq (q^2/mc^2)^{-1} = 0.64 \times 10^{16}$ cm^{-1}. Therefore,

most of the protons of the pulse must be concentrated within a 10 cm axial length in order to have a field reversal factor $\eta \approx 120\%$. However, it should be emphasized that the rigid-rotor model overestimates the number of charged particles required for field reversal because the azimuthal current density in this model peaks at the outer edge of the beam. In contrast, the current density in the experiments peaks near the inner edge of the beam, as may be seen from Fig. 15.

Computer simulation of the experiment using the measured voltage and total current and assuming that the current efficiency of the IRT is 30% show that the ratio of the self to the applied magnetic field at 60 cm after the cusp (position of B_{z2} probe) is 1.44. The radially inward motion of the beam has been simulated by assuming the protons at the outer edge of the pulse arrive at the anode with a negative radial velocity which is the 1/10 of their total velocity.

The slow decay of signals of the B_{z2} and B_{z3} probes (Fig. 13) is probably associated with the plasma formed on the surface of the long probes. This is supported by the observation that the decay of signals of small B_z probes that are inserted radially is substantially faster than that of the long multi-probe. Assuming exponential decay of the probe signals, i.e., $B(t) = B(t_o) \exp[-(t - t_o)R/L]$ and that the plasma formed on the surface of the glass probe expands with an average speed of about 2 cm/μsec, it has been estimated that the plasma resistivity is about 1.5×10^{-2} Ω-cm. For such a resistivity Spitzer's formula gives an electron plasma temperature $kT_e = 1.6\ Z^{2/3}$(ev), which is not unexpected. Although the plasma formed on the housing of the magnetic probe can explain the slow decay of the probe signals, it cannot account for an appreciable

fraction of the observed diamagnetism. A plasma energy density of 1.4×10^4 J/m^3 is necessary to generate the observed self magnetic field of 1.87 KG shown in Fig. 13.

It is rather unlikely that more than 10^{16} protons of average energy 1 MeV strike the 1.6 cm diameter, 1m long glass housing of the magnetic probe over 25 nsec, i.e., when the peak of B_{z2} signal occurs. Therefore, the energy available to form the plasma does not exceed 1.6 KJ. For normal incidence, the range of 1 MeV protons on pyrex is about 20μm. Since $v_\theta/v_z \approx 1/5$, the protons strike the probe housing at an angle that is appreciably greater than zero and therefore their effective range is taken as 10μm. Consequently, the 1.6 KJ energy of the protons is deposited in ~ 1.12 grams of glass. The energy required to raise the temperature of 1.12 gm of glass to boiling point is about 1.9 KJ. Therefore, it is unlikely that a high density plasma is formed on the housing of the probe.

A similar conclusion is reached from the peak proton power density striking the probe. This power density is estimated to be less than 0.15 GW/cm^2. Since the interaction of a proton beam with glass is similar to the interaction of a proton beam with an aluminum target, it may be concluded from Fig. 6 of Tucker[23] et al that for such low power density the interaction is "direct", i.e., the absorbed beam energy on the target does not change permanently its material structure but rather excites an elastic stress pulse.

It is doubtful that there is an appreciable number of electrons that has axial velocity and total energy comparable to that of the

protons. No light is observed by an image intensifier camera operated in the frame mode when the beam strikes a lucite plate covered with 30μm aluminum foil. In contrast, when the thickenss of aluminum is reduced to below 6μm the lucite target that is located 120 cm from the cusp emits strongly. Note that for normal incidence the range of 1 MeV electrons in aluminum is 1800μm and that of protons of the same energy is 13μm.

In contrast to axial fields, the azimuthal field of the layer appears to be almost zero before the cusp and very small in the uniform field region. Figure 16 shows the output of a B_θ probe that is located 77 cm beyond the midplane of the cusp at 0.5 cm from the wall of the vacuum chamber. Typically, the B_θ field at this position is less than 100 G.

4. Conclusions

The achieved transient field reversal with a rotating proton layer is an important step toward the objective of our program which is the formation of a trapped, field reversed ion ring.

Presently, our effort is concentrated in reducing the "filling-in" of the hollow beam by suitably reshaping the anode and cathode electrodes. A beam with small inward radial velocity and thus less "filling-in" will allow the insertion of a cusp sharpening ferromagnetic disc resulting in a shorter cusp transition width. This, will make possible the operation of the system in higher magnetic fields, thus achieving higher velocity ratios v_θ/v_z without appreciable losses at the cusp.

The trapping studies of the proton pulse, using the original configuration,[24] will start immediately after the successful increase of the ratio v_θ/v_z. This has the advantage that the field lines of

the ramp shaped field will not intersect the walls of the converging vacuum chamber and thus most of the particle losses in this section of the system will be eliminated.

Table I

Azimuthal current required to generate B_o = 1.8 KG at the center of a coil of length 2L, inner radius a_1 and outer radius a_2.

a_1	a_2	2L	$\frac{B_o}{\mu_o J a_1}$	J(A/cm^2)	I(KA)
3	15	18	2.87	166	35.9
5	15	20	1.43	200	40.0
5	15	30	1.66	173	51.8
7.5	7.5	30	0.80	239	53.7
7.5	15	15	0.56	341	38.4

References

1. R.F. Post, Fourth Intern. Conf. on Driven Magnetic Fus. Reactors, Erice, Italy, Sep., 18-26, 1978.

2. NC. Christofilos, Proc. 2nd Int. Conf. on the Peaceful Uses of Atomic Energy, Geneva, 1958, 32, 279 (1958).

3. N.C. Christofilos, et al., Proc. 4th Intern. Conf. in Plasma Physics and Contrciled Nucl. Fus. Research, Madison, 1971, IAEA 1, 119 (1971).

4. T.J. Bzura et al., Phys. Rev. Lett. 29, 256 (1972); H.A. Davis et al., Phys. Rev. Lett. 37, 542 (1976).

5. N.C. Christofilos, U.S. Patent #3,664,921.

6. J. Rand McNally, Jr., Oak Ridge Nat. Lab. Report #ORNL-TM-4965 (1975).

7. T.C. Simonen et al. 7th IAEA Conf. on Plasma Physics and Contr. Fus. Research, paper CN-37-J-1, Innsbruck, Austria, Aug. 23-30, 1978.

8. C.A. Kapetanakos, J. Golden and W.M. Black, Phys. Rev. Lett., 37, 1936 (1976).

9. J. Golden, C.A. Kapetanakos, S.J. Marsh and S.J. Stephanakis, Phys. Rev. Lett., 38, 130 (1977).

10. J.A. Pasour, R.A. Mahaffey, J. Golden and C.A. Kapetanakos, Phys. Rev. Lett., 40, 448 (1978); J.A. Pasour, R.A. Mahaffey, J. Golden and C.A. Kapetanakos, NRL Report #4103 (1979).

11. D.S. Prono, J.W. Shearer and R.J. Briggs, Phys. Rev. Lett 37, 21 (1976).

12. S.J. Stephanakis, D. Mosher, G. Cooperstein, J.R. Boller, J. Golden, and S.A. Goldstein, Phys. Rev. Lett. 37, 1543 (1976).

13. J. Maenchen, L. Wiley, S. Humphries, Jr., E. Peleg, R.N. Sudan and D.A. Hammer, Phys. Fluids 22, 555 (1979).

14. D.J. Johnson, G.W. Kuswa, A.W. Farnsworth, Jr., J.P. Quintenz, R.J. Leeper, E.J.T. Burns and S. Humphries, Jr., Phys. Rev. Lett. 42, 610 (1979).

15. C.A. Kapetanakos, J. Golden, R.A. Mahaffey, S.J. Marsh and J.A. Pasour, to be published in the Proc. of the 3rd Intern. Top. Conf. on High Power Electron and Ion Beam Research and Technology Novosibirsk, USSR, July 3-6, 1979.

16. S.J. Marsh, Adam Drobot, J. Golden and C.A. Kapetanakos, Phys. Rev. Lett., 39, 705 (1977); also Phys. of Fluids 21, 1045 (1978).

17. See, for example, L.E. Thode, B.B. Godfrey and W.R. Shanahan, Phys. Fluids, 22, 747 (1979) and references therein.

18. W. Hintze, private communcation.

19. R.B. Miller and D.C. Straw, J. Appl. Phys. 47, 1897 (1976).

20. F.C. Young, J. Golden and C.A. Kapetanakos, Rev. Sci. Instrum. 48, 432 (1977).

21. J. Golden, R.A. Mahaffey, J.A. Pasour, F.C. Young and C.A. Kapetanakos, Rev. Sci. Instrum. 49, 1384 (1978).

22. C.A. Kapetanakos, J. Golden and K.R. Chu, Plasma Physics 19, 387 (1977).

23. T.R. Tucker, D. Mosher and D. Hinshelwood, NRL Report #4043 (1979).

24. C.A. Kapetanakos, J. Golden, Adam Drobot, R.A. Mahaffey, S.J. Marsh and J.A. Pasour, Proc. of the 2nd Intern. Top. Conf. on Electron and Ion Beam Research and Technology, Ithaca, NY Oct. 3-5 1977, v. 1, p. 435.

Acknowledgements

We are grateful to F.C. Young for providing to us the data on the calibration of γ-ray detector, to A.E. Robson for very helpful discussions and to R. Covington for his technical assistance.

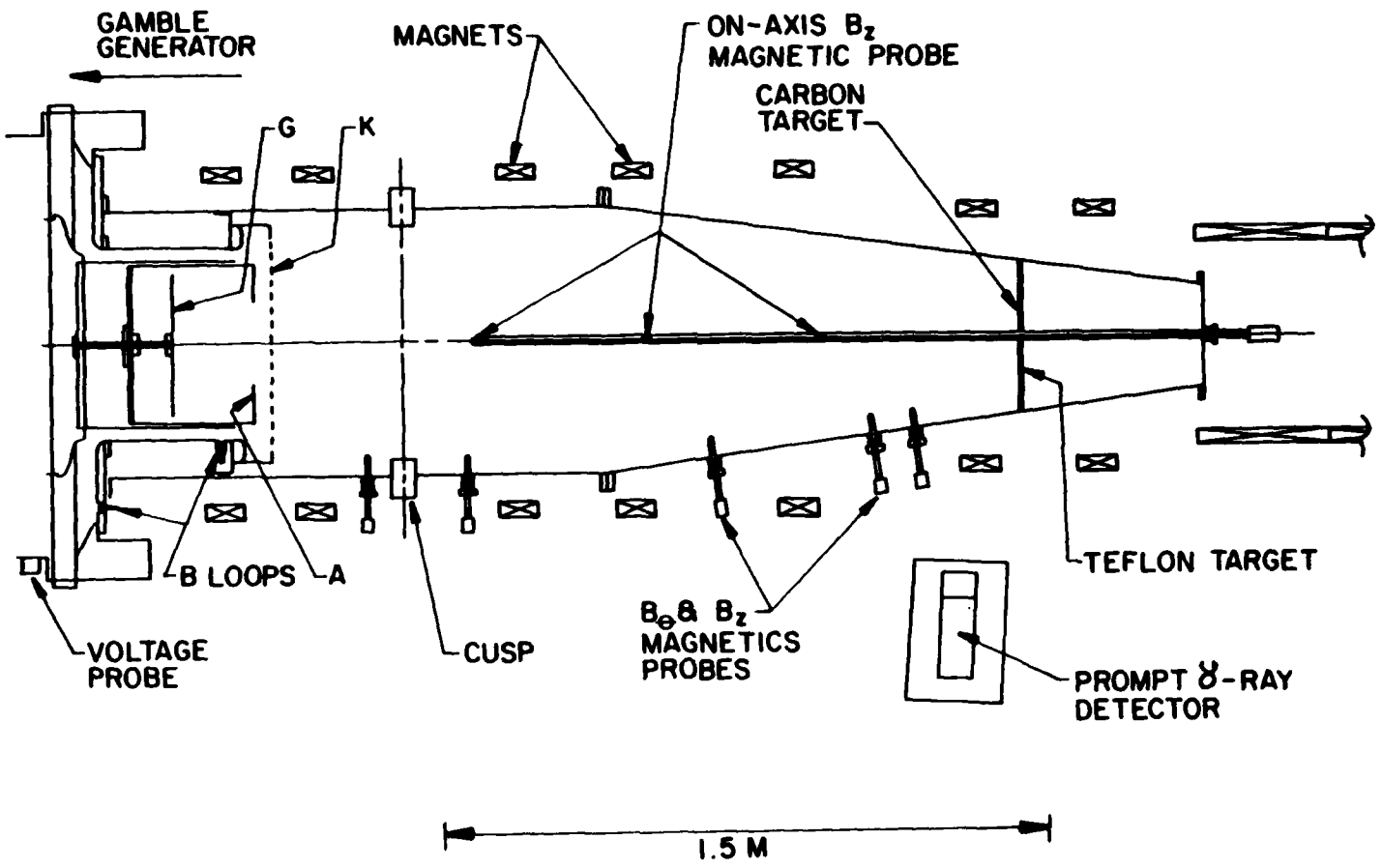

Fig. 1 — Schematic of a section of the NRL Ion Ring Experiment in which the series of experiments that are described in this report have been performed

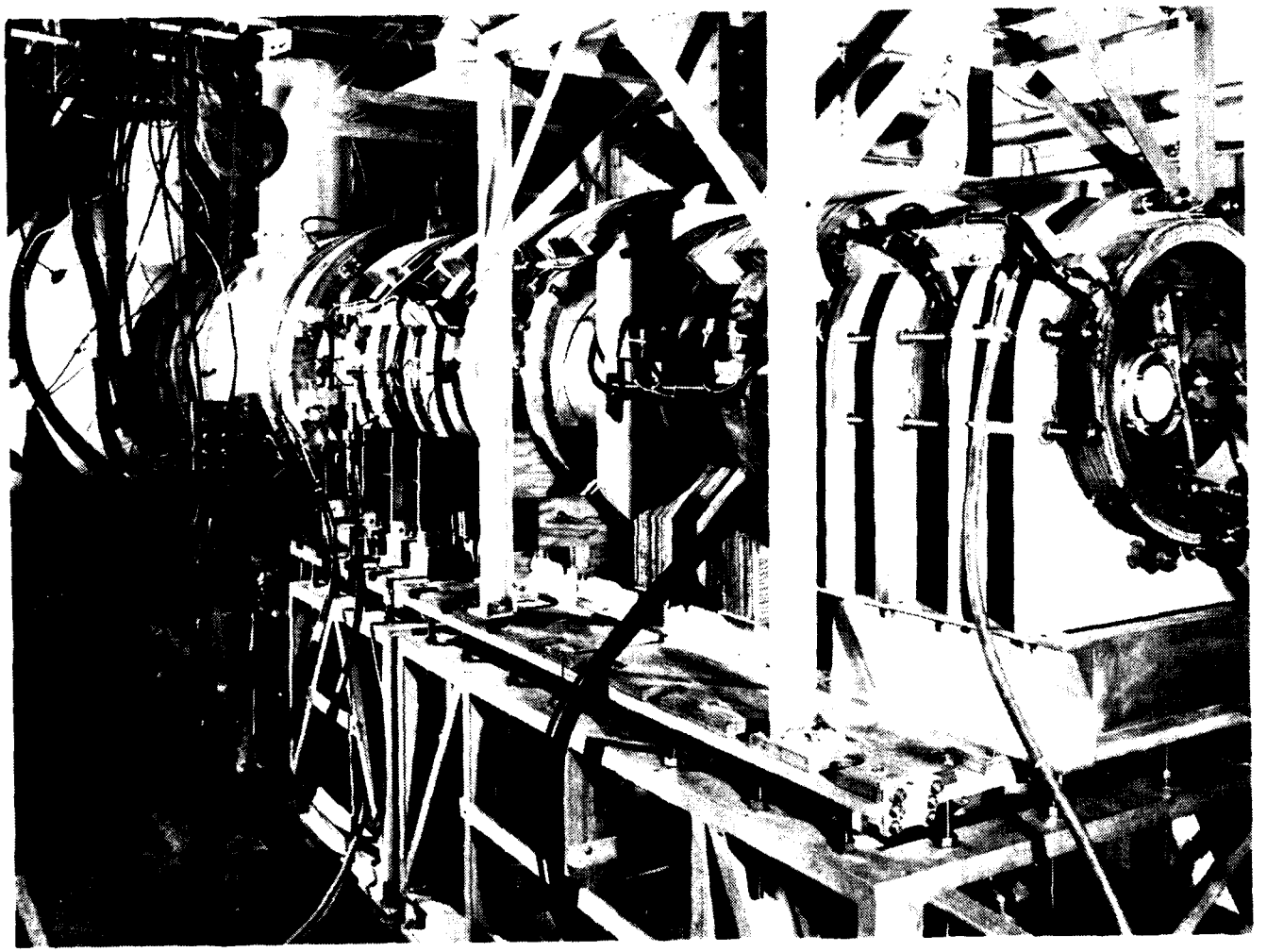

Fig. 2 — Photograph of the same section of the experimental apparatus

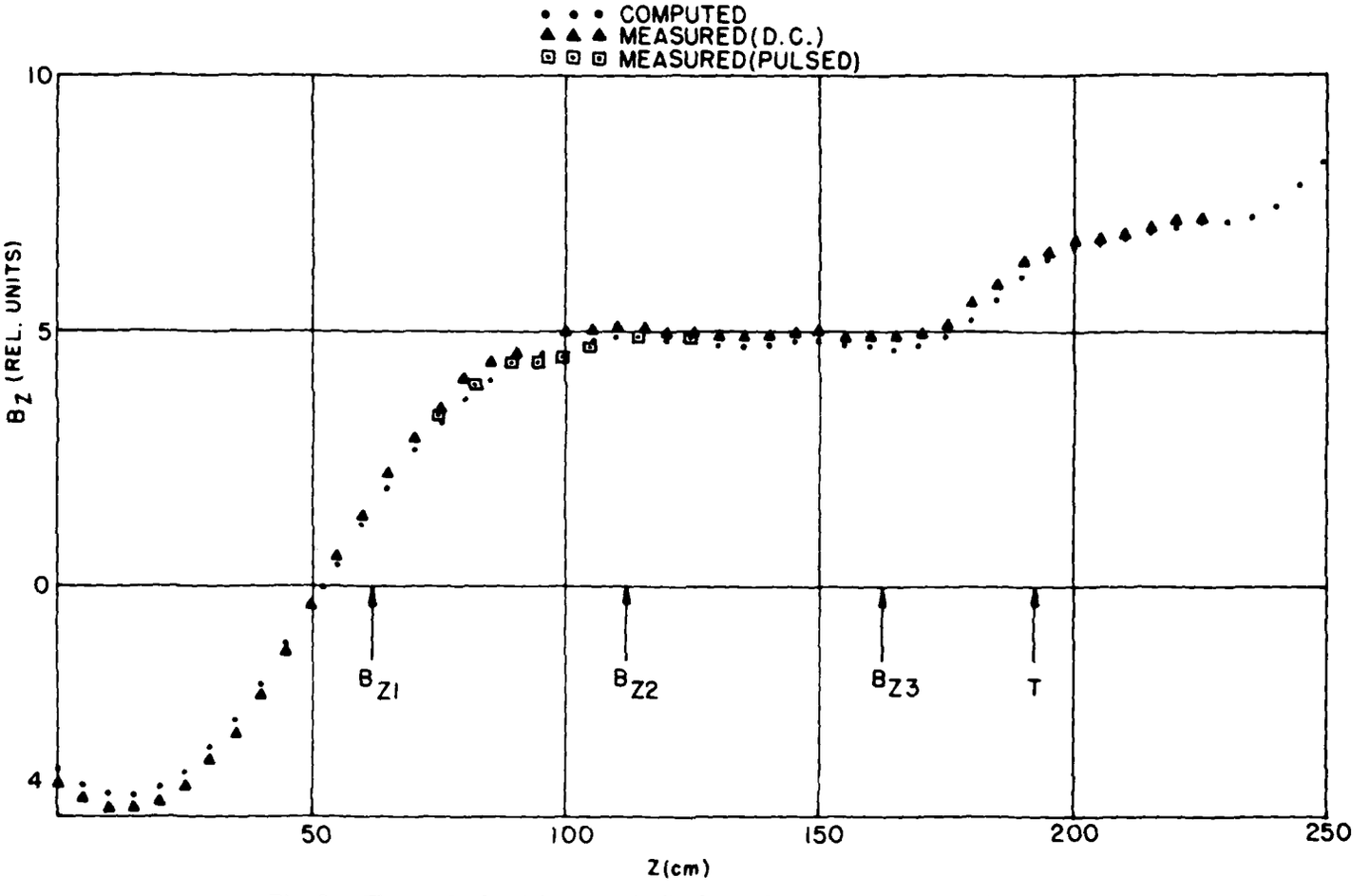

Fig. 3 — The applied axial magnetic field as a function of axial position

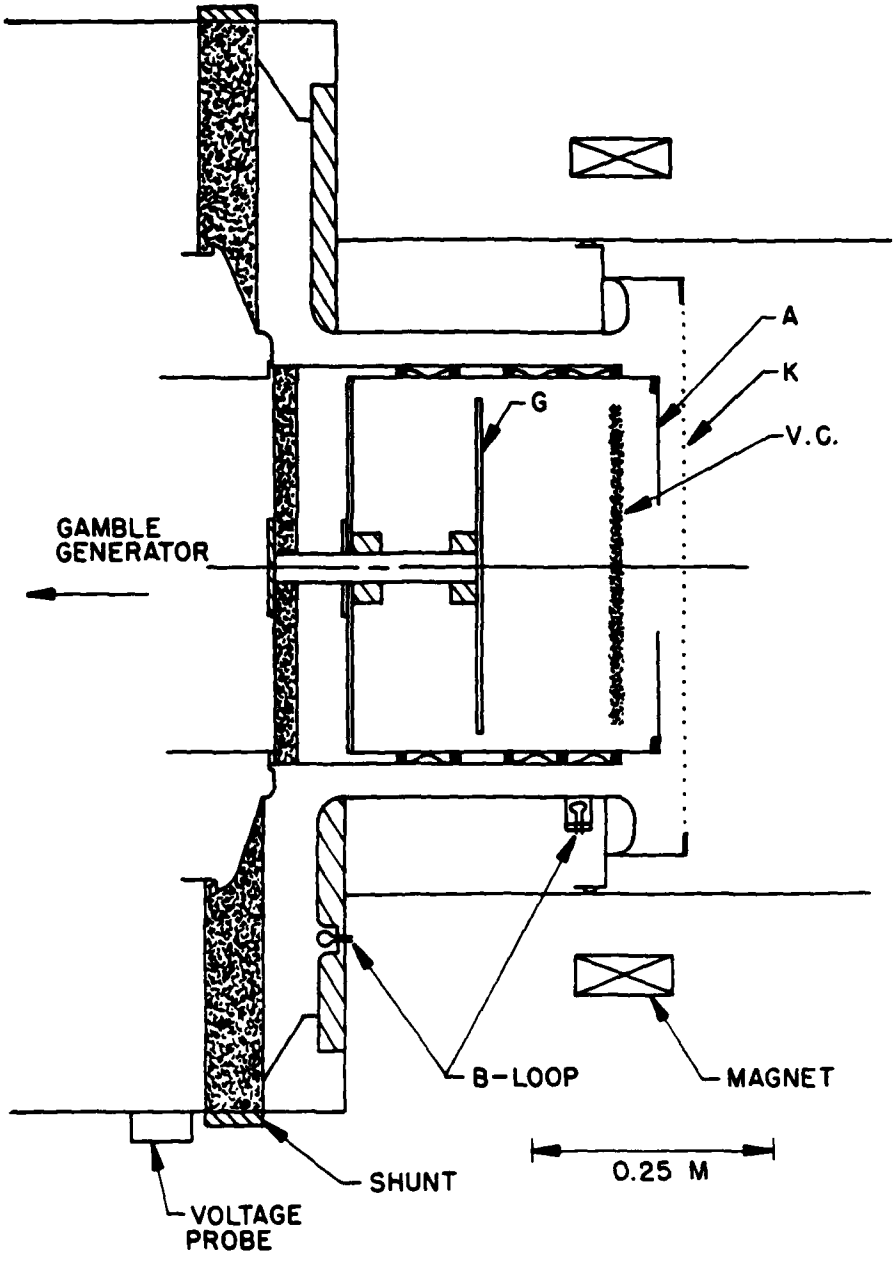

Fig. 4 — A schematic of the Inverse Reflex Tetrode. Shown are the grid (G), virtual cathode (V.C.), anode (A), and cathode (K).

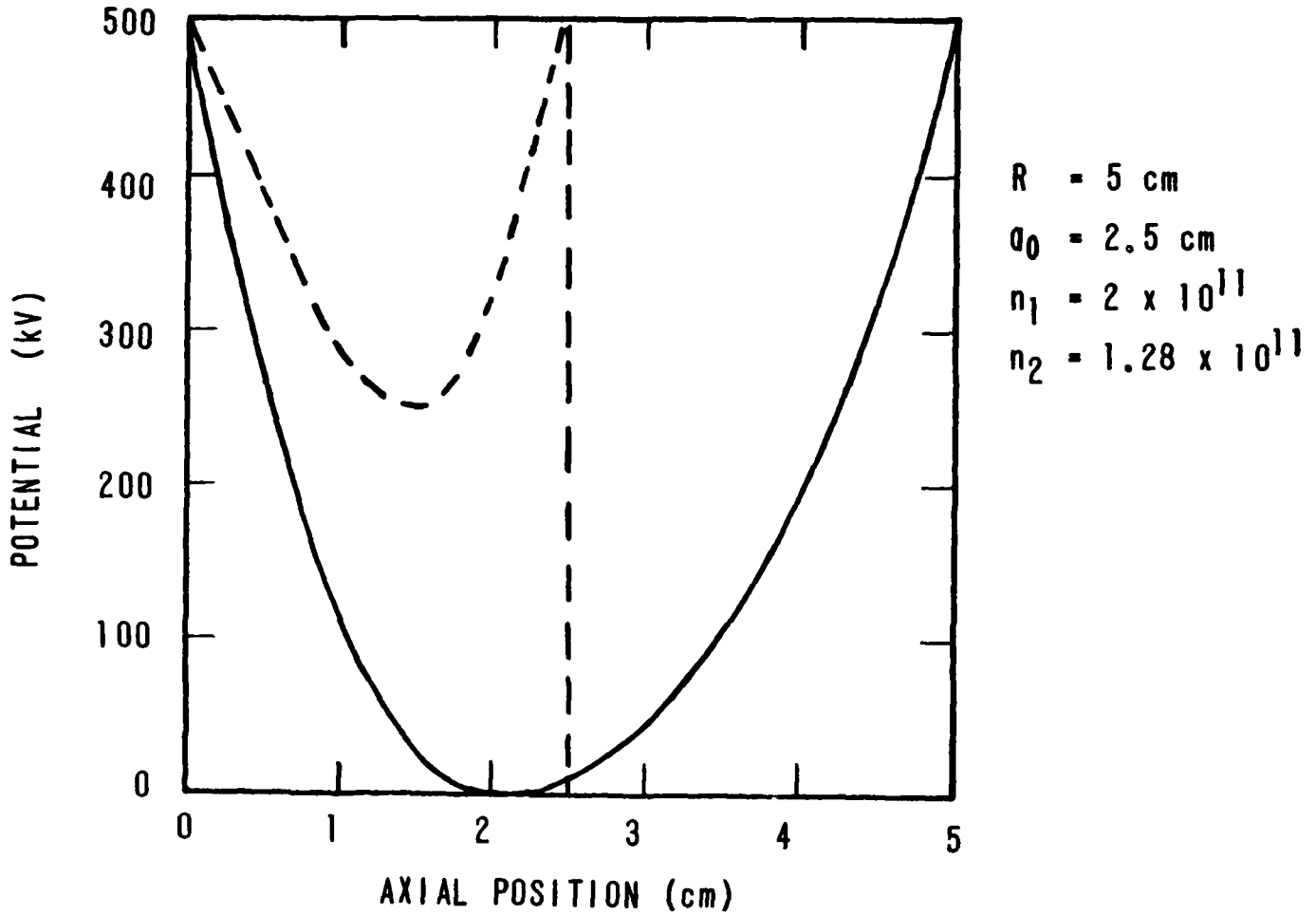

Fig. 5 — The potential distribution between the anode A (located at axial position = 0) and the grid G of an IRT. The solid (dashed) curve is for an A-G spacing = 5 (2.5) cm.

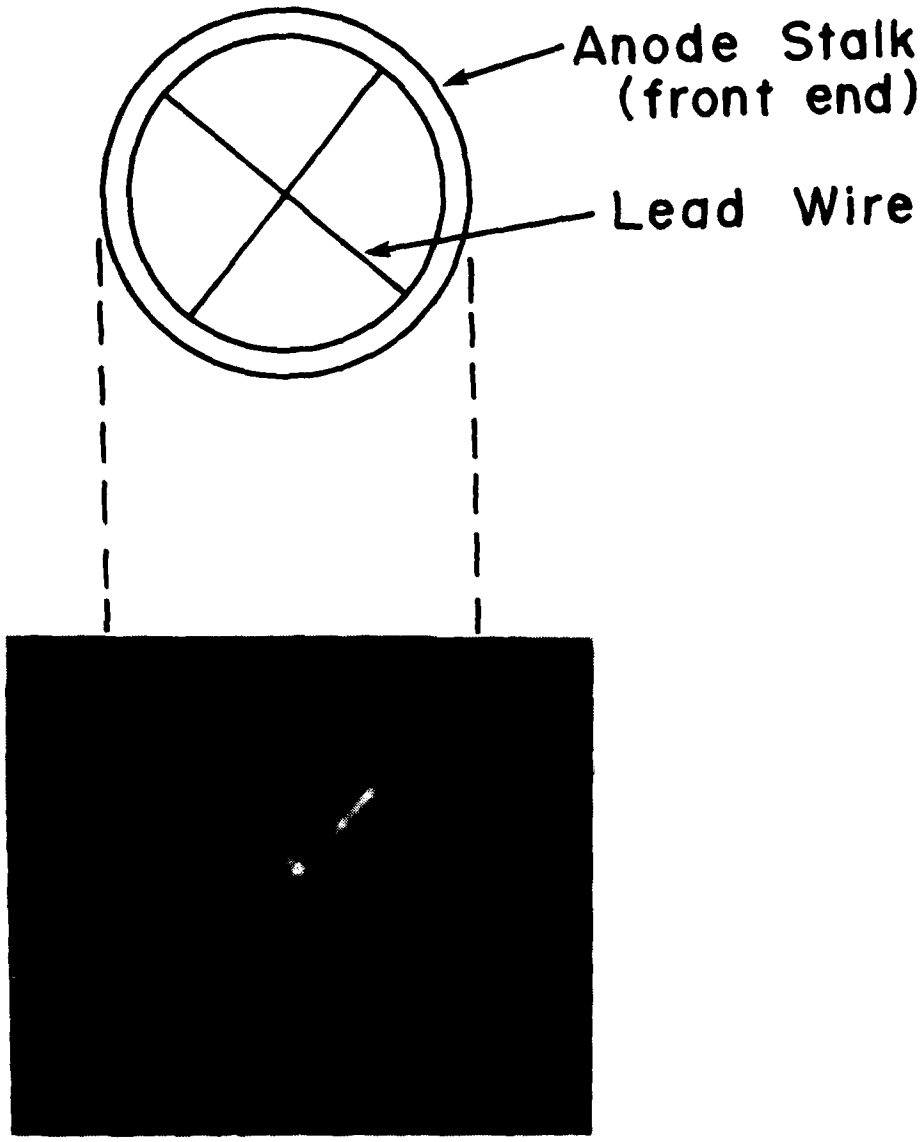

X-Ray Pinhole Photograph

Fig. 6 — X-ray pinhole photograph of two crossed lead wires mounted inside the anode stalk, about 15 cm from the anode

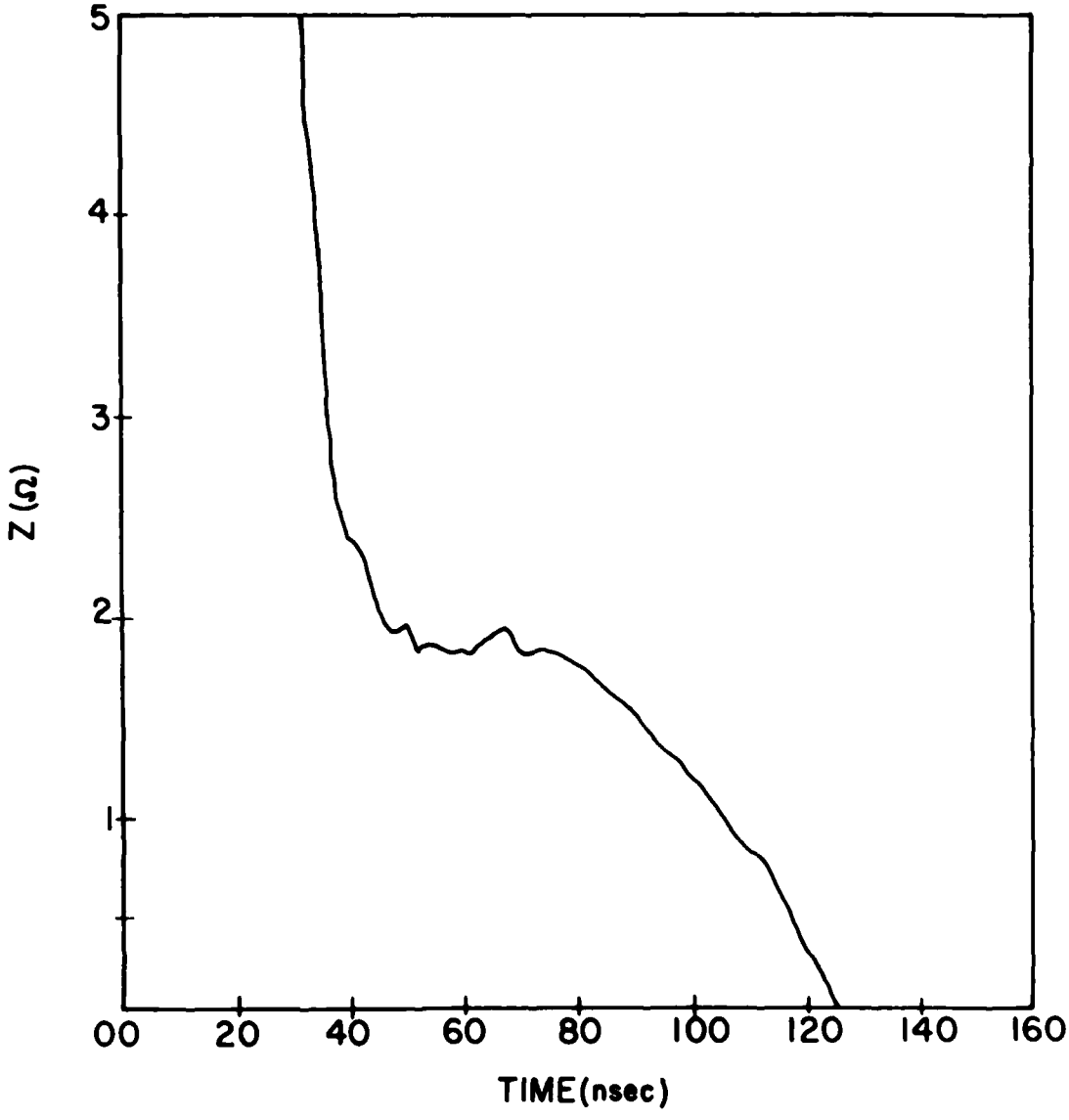

Fig. 7 — The impedance Z of the IRT as a function of time

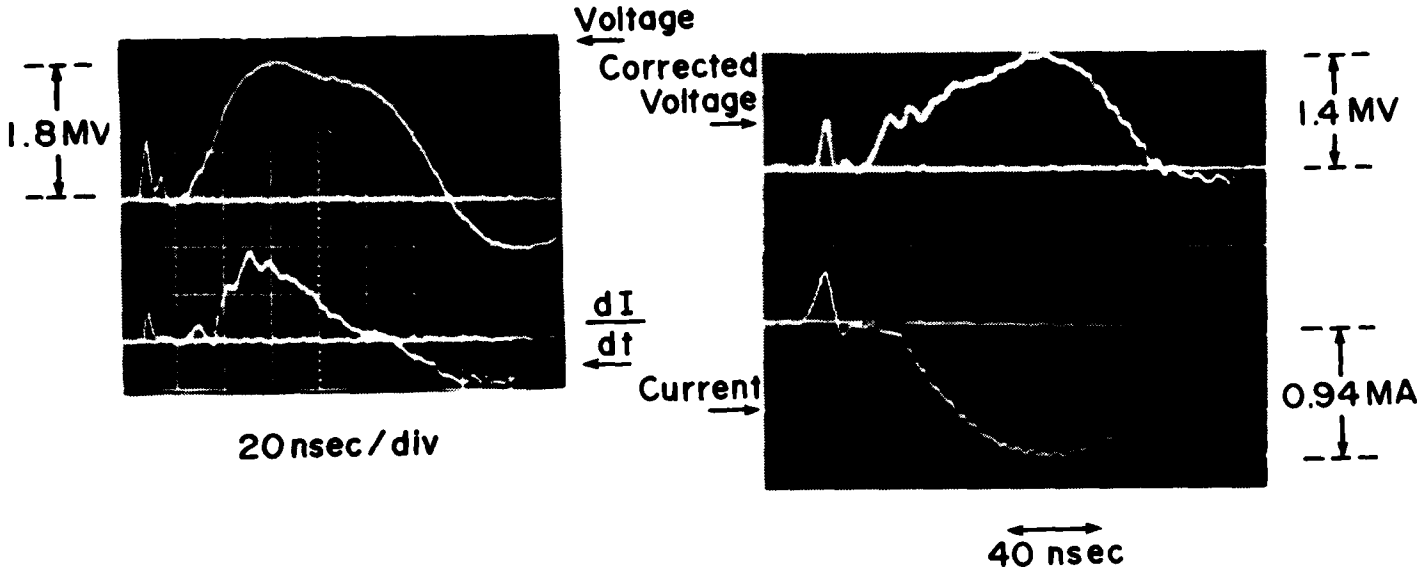

Fig. 8 — Typical waveforms of the total diode voltage, the time derivative of the total current, the inductively corrected voltage, and the total current for the IRT

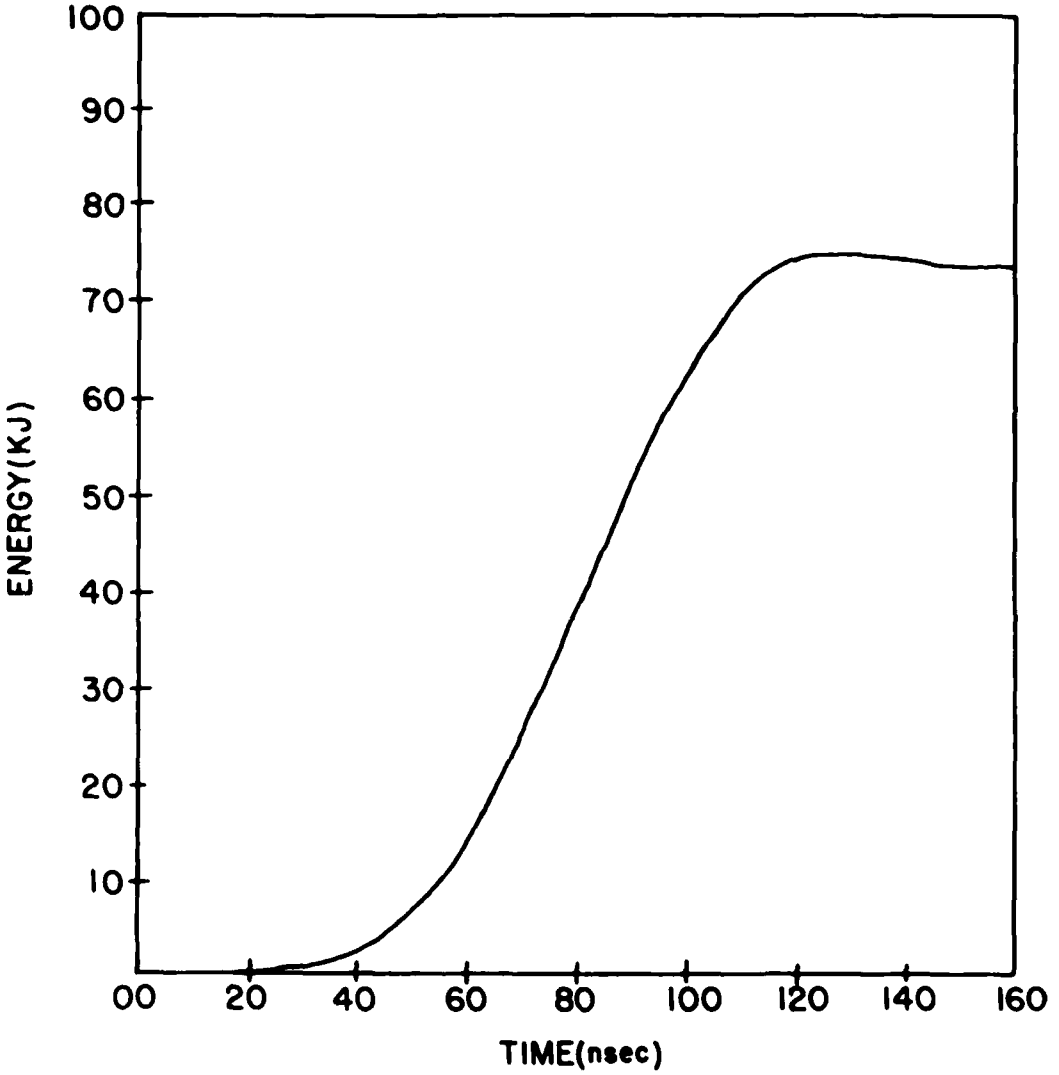

Fig. 9 — The energy coupled to the IRT as a function of time

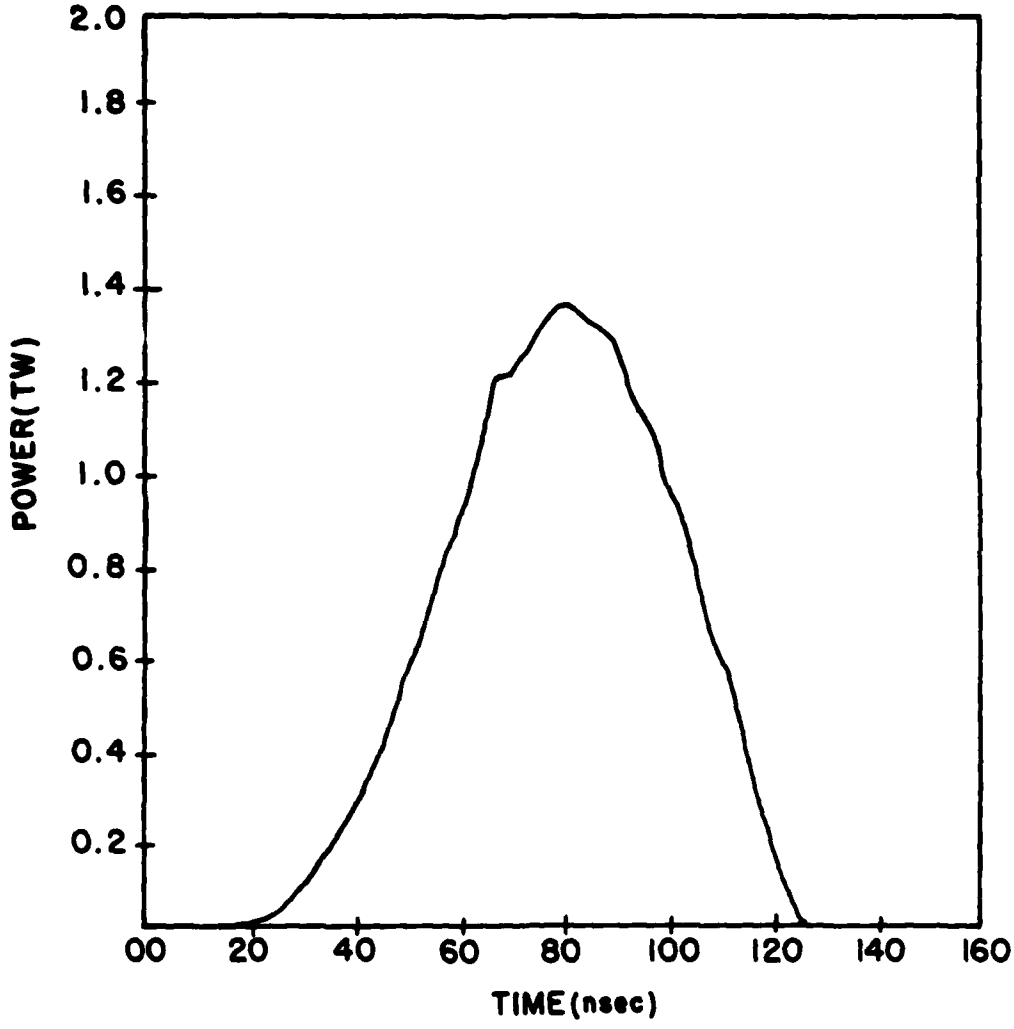

Fig. 10 — Power delivered by the generator to the IRT as a function of time, when the Marx of the upgraded Gamble II generator is charged to 38 KV, i.e., to only 63% of its maximum designed voltage.

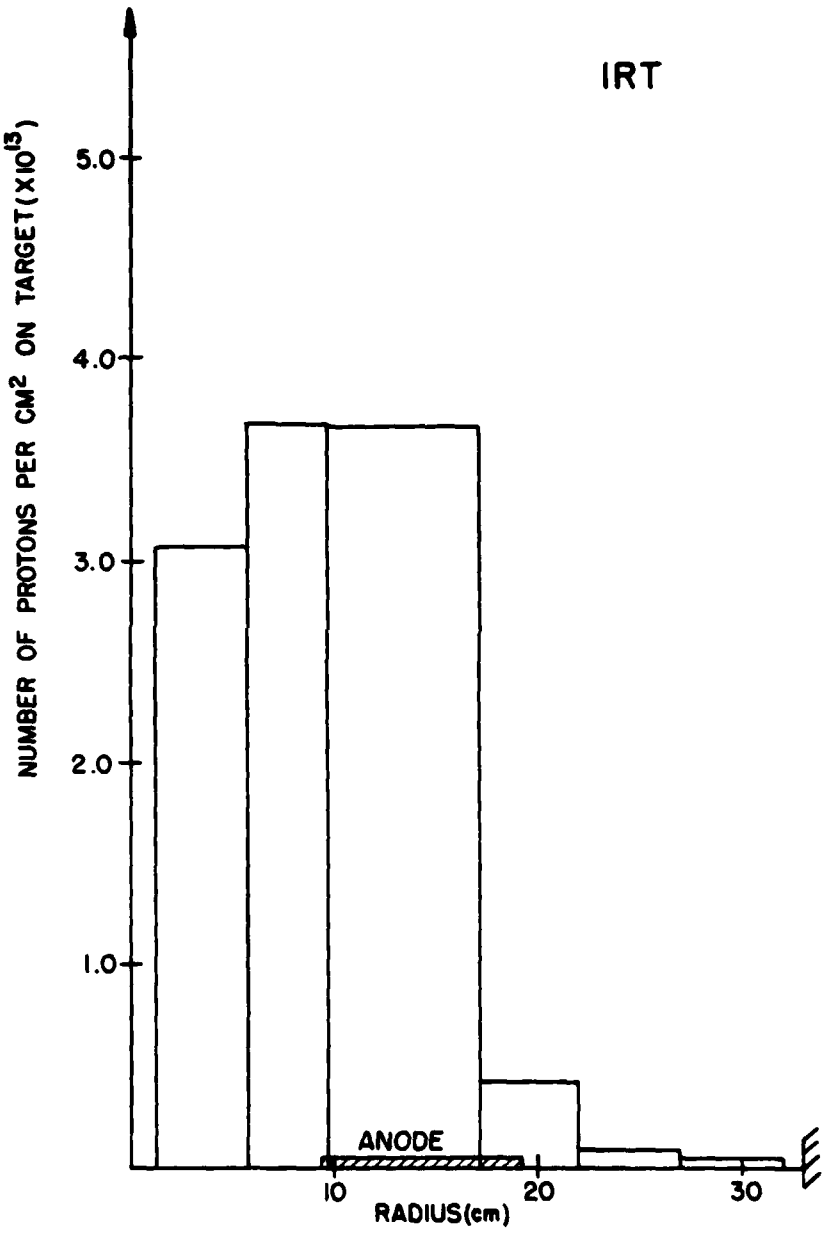

Fig. 11 — The proton dose versus radius at 15 cm downstream from the anode

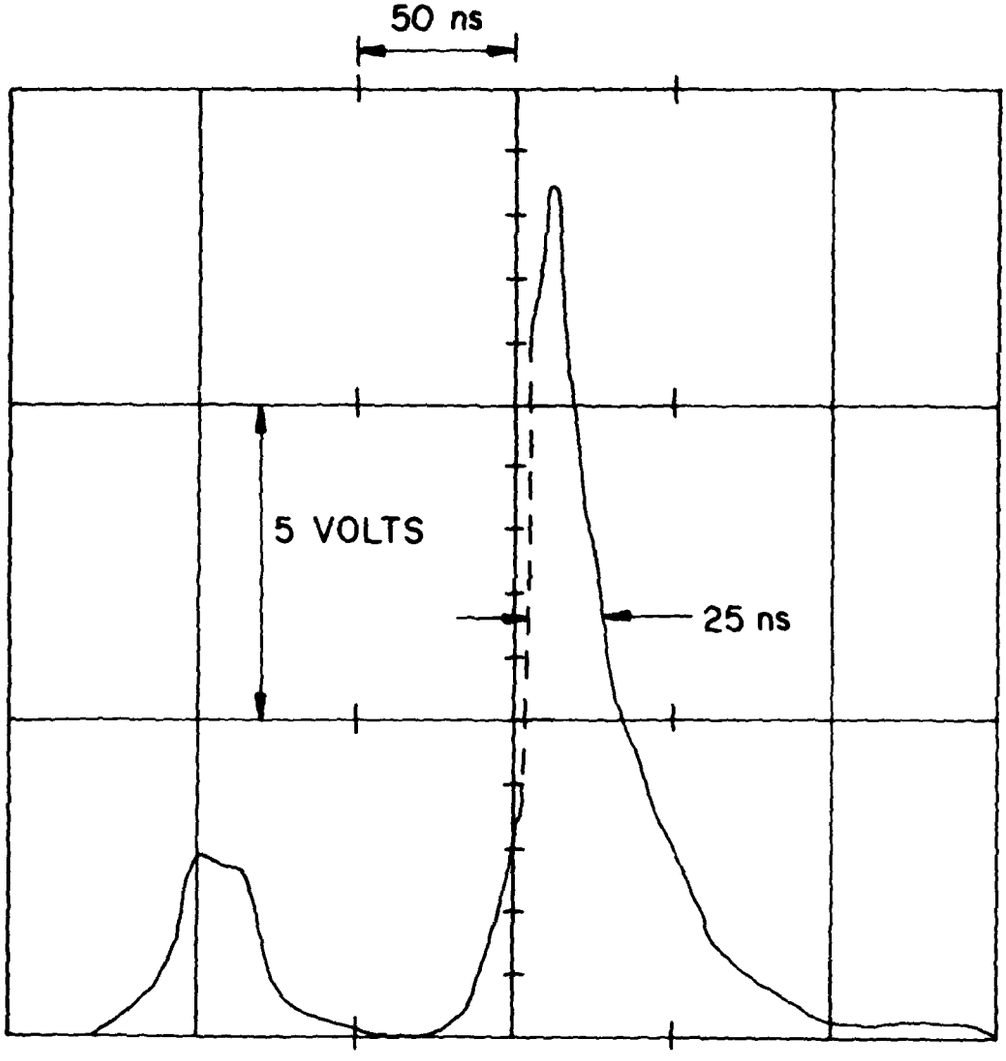

Fig. 12 — The prompt γ-ray signal (second peak) as a function of time produced by the proton beam via the $^{19}F(p,\alpha\gamma)^{16}O$ reactions induced in a teflon target located at z = 190 cm.

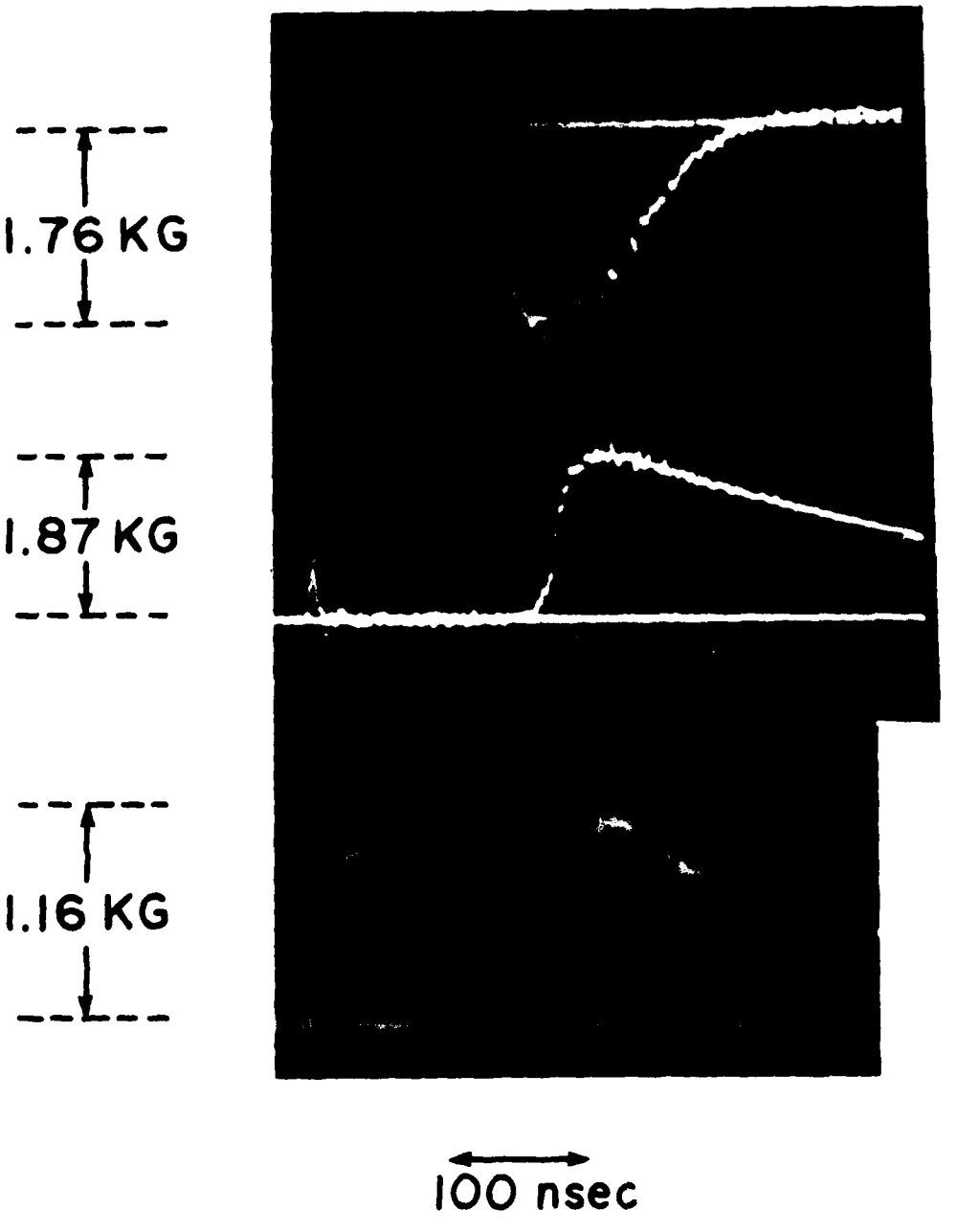

Fig. 13 – Diamagnetic signals measured by on-axis probes at (upper) 10, (middle) 60, and (lower) 110 cm downstream from the cusp

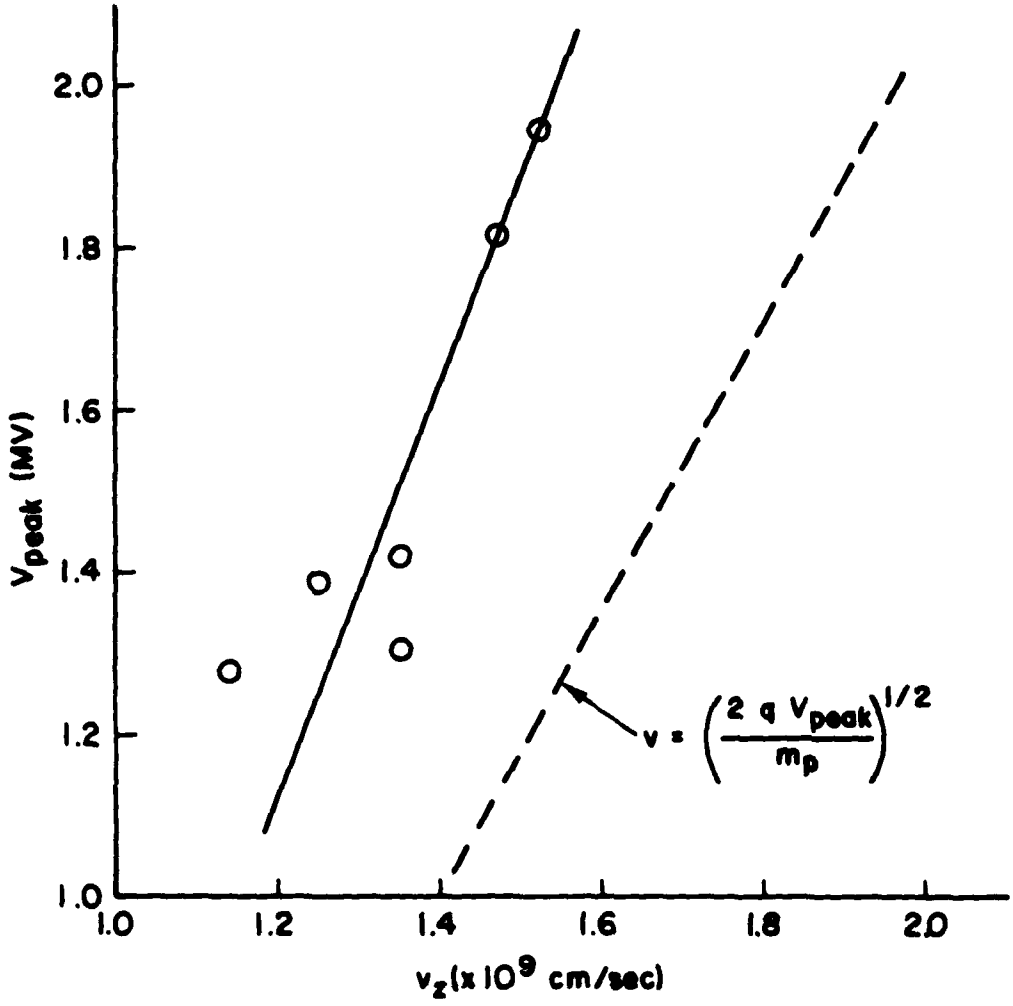

Fig. 14 — The solid line gives the observed axial velocity of the proton pulse in the uniform magnetic field as a function of the peak applied voltage on the anode. The dashed line gives the velocity corresponding to the peak voltage.

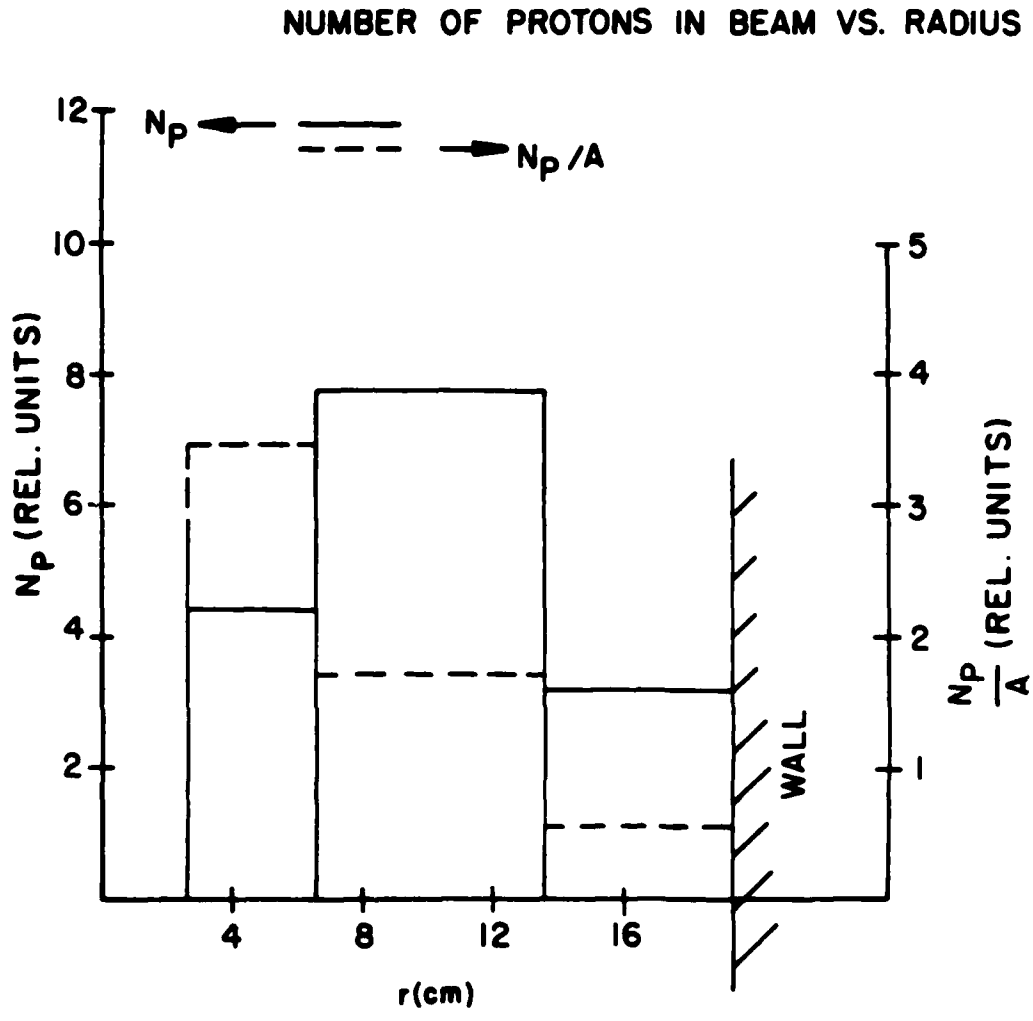

Fig. 15 — Radial profiles of the proton pulse 145 cm after the cusp

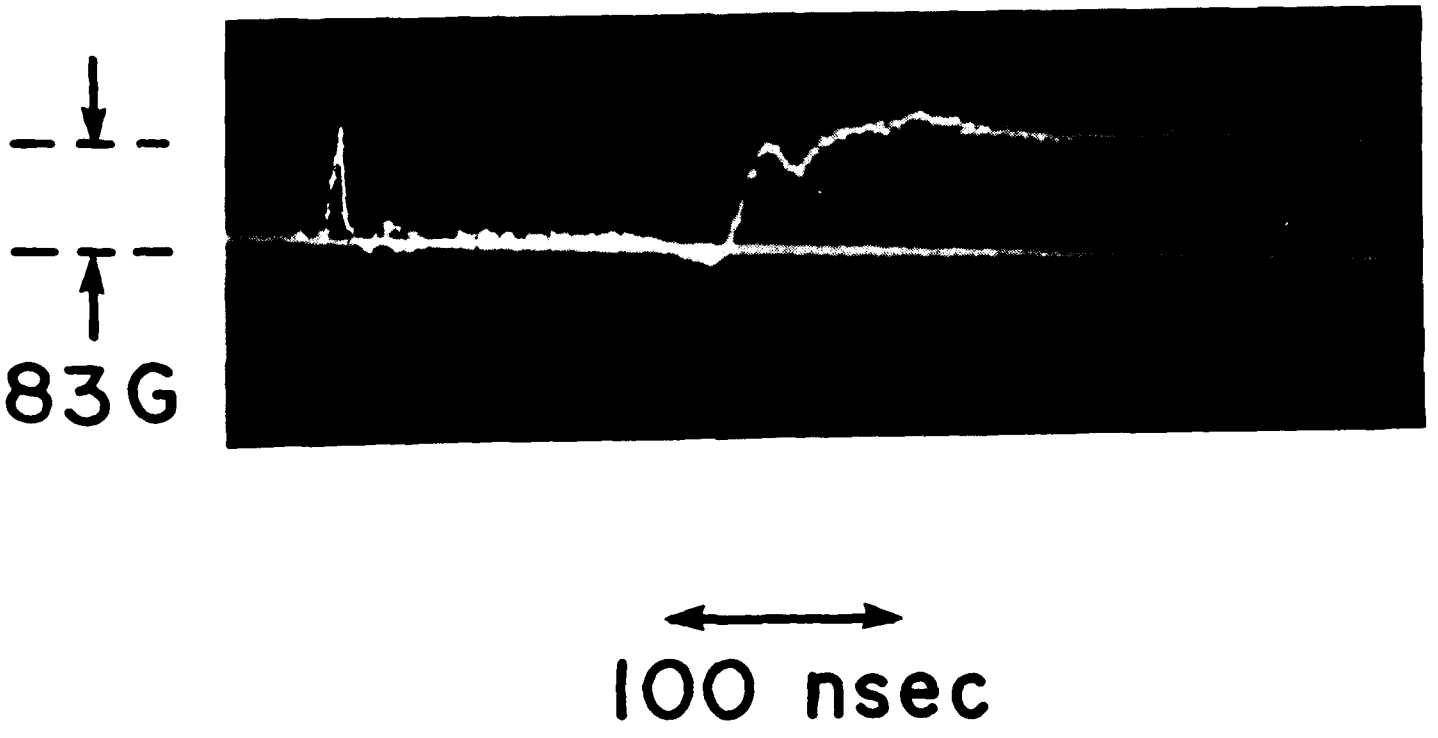

Fig. 16 — The azimuthal magnetic field of the beam versus time at a radius = 30.9 cm and an axial position 77 cm from the cusp. The "crowbaring" of the signal is attributed to plasma formation on the probe.